Vol. 389: 17–29, 2009
doi: 10.3354/meps08175

MARINE ECOLOGY PROGRESS SERIES
Mar Ecol Prog Ser

Published September 4

Microbial carbon monoxide uptake in the St. Lawrence estuarine system

Huixiang Xie[1,*], Yong Zhang[1,2], Karine Lemarchand[1], Patrick Poulin[1]

[1]**Institut des Sciences de la Mer, Université du Québec à Rimouski, 310 allée des Ursulines, Rimouski, Québec G5L 3A1, Canada**

[2]***Present address:*** **Yantai Institute of Coastal Zone Research for Sustainable Development, Chinese Academy of Sciences, 17 Chunhui Road, Laishan District, 264003 Yantai, PR China**

ABSTRACT: Microbial uptake of carbon monoxide (CO) in the Gulf of St. Lawrence and the estuary of the St. Lawrence River, Canada, typically followed first-order kinetics at ambient CO concentrations, [CO], but saturation kinetics occasionally occurred in spring. The first-order uptake rate constant, K_{co}, decreased from the upper estuary (8.48 d^{-1}) to the lower estuary (3.94 d^{-1}) and the gulf (1.32 d^{-1}). K_{co} inversely varied with tide and decreased from its highest value in summer (7.52 d^{-1}) to intermediate values in spring (5.15 d^{-1}) and autumn (4.12 d^{-1}), and to its lowest value in winter (1.09 d^{-1}). Maximum K_{co} values always occurred in a turbidity maximum zone near the head of the estuary. An empirical model was proposed to account for the effect of particle-associated bacteria on K_{co}. Temperature dependence of K_{co} obeyed Arrhenius behavior with the activation energy being lower in the upper estuary (21.5 kJ mol^{-1}) than in the lower estuary and gulf (32.7 kJ mol^{-1}). The combination of bacterial abundance and temperature can serve as an all-season predictive tool for K_{co}. CO uptake rate versus [CO] plots show typical Michaelis-Menten kinetics or inhibition behavior at elevated [CO]. K_m was low and relatively invariable: 3.2 nmol l^{-1} [CO] in autumn and 4.9 nmol l^{-1} [CO] in winter. CO specific affinity in autumn (1.25 l (mg of cell)$^{-1}$ h^{-1}) more than doubled that observed in winter (0.51 l (mg of cell)$^{-1}$ h^{-1}). This study demonstrated strong seasonal variations in microbial CO uptake and complex influences of various biotic and abiotic variables on this process.

KEY WORDS: Carbon monoxide · Microbial uptake · Seasonal variation · Temperature dependence · Bacteria · Suspended particles · Estuarine waters · Gulf of St. Lawrence

INTRODUCTION

Microbial oxidation is usually the dominant sink of carbon monoxide (CO) in oceanic waters and thereby controls the amplitude of the diurnal cycles of CO in the upper layers of ocean waters (Conrad et al. 1982, Bates et al. 1995, Zafiriou et al. 2003, 2008). The fast microbial removal renders only a minor (~14%) portion of CO in seawater, which is produced mainly by photolysis of colored dissolved organic matter (Conrad et al. 1982), to be exchanged to the atmosphere (Zafiriou et al. 2003). Biological CO oxidation also potentially influences the flow of organic C in the marine food web and the respiratory CO_2 budget by serving as a supplemental energy source for the CO-oxidizing organisms (Moran & Miller 2007). CO oxidation is carried out by an unexpected diversity of marine bacteria (Tolli et al. 2006, King & Weber 2007, Moran & Miller 2007) and genome-sequencing of the CO-oxidizer *Silicibacter pomeroyi* (Moran et al. 2004) has greatly enhanced the understanding of this process at both the molecular and ecological levels. Despite these recent insights, the species-level identity of other CO-oxidizing microbes remains elusive, as does our comprehension of its metabolic functions. The roles of microbial CO oxidation in regulating the fate of marine organic carbon and CO air–sea exchange also need to be better defined, as their current flux estimates are based on limited data (Zafiriou et al. 2003, Moran & Miller 2007). This requires more extensive spatial and temporal mapping of microbial CO uptake rates and the development of predictive tools for the uptake rates based

*Email: huixiang_xie@uqar.qc.ca

on relatively easily obtainable biotic and abiotic variables.

Microbial CO uptake is expected to vary seasonally due to changes in such factors as bacterial cell abundance and species composition, water temperature (T) and supply of nutrients. Butler et al. (1987) have reported the only 4-season microbial CO uptake turnover times, which were obtained from Yaquina Bay, Oregon, but gave no details of the CO uptake seasonality and its possible links to other environmental variables. Moreover, the ^{14}C technique they employed may not adequately characterize the CO uptake kinetics when ambient CO concentration, [CO], is high or large amounts of ^{14}C-labelled CO are added (Tolli & Taylor 2005, Xie et al. 2005, 2009). Although temperature is a well-known key factor that controls bacterial activity in general (e.g. Shiah & Ducklow 1994), the extent of T-dependence of microbial CO uptake remains unclear. Recent findings reveal that ambient seawater CO concentration can also influence microbial CO uptake kinetics as a result of unexpectedly high enzymatic affinities for CO expressed by CO-oxidizing bacteria (Tolli & Taylor 2005, Xie et al. 2005, 2009). While CO uptake generally follows or can be approximated as first-order kinetics at low ambient [CO], mixed-order, saturation or even inhibition kinetics can occur at elevated [CO] (Zafiriou et al. 2003, 2008, Xie et al. 2005, 2009). The latter requires Michaelis-Menten kinetics to derive limiting rates, V_{max}, and half-saturation substrate concentrations, K_m, that more accurately characterize this process. Data in the literature on V_{max} and K_m of microbial CO uptake are scarce and cover only limited seasons and areas (salinity usually >28) (Tolli & Taylor 2005, Xie et al. 2005, 2009). Evidently, more Michaelis-Menten kinetics studies are needed to characterize CO consumption on larger salinity and seasonal scales. In a cross-system assessment encompassing warm, cold (Arctic), coastal and open ocean waters, Xie et al. (2005) have demonstrated that the first-order rate constant of microbial CO uptake (K_{co}) positively correlates with chlorophyll *a* concentration, [chl *a*], a proxy of primary productivity. This correlation is, however, based only on summer data in warm waters and autumn data in Arctic waters. The Arctic spring data acquired later failed to support this relation, thus invalidating [chl *a*] as an all-season indicator for K_{co} in the Arctic (Xie et al. 2009).

The present study goes beyond previous investigations to examine a high mid-latitude estuarine system: the Gulf of St. Lawrence and the estuary of the St. Lawrence River, Canada. It reports a 4-season K_{co} dataset, the first assessment of the T-dependence of K_{co}, and a 2-season probe of the Michaelis-Menten CO uptake kinetics. The relationships between K_{co} and various biotic and abiotic variables were elaborated. Results from this work shed new insights into CO microbiology, aid in refining regional and global microbial CO uptake rates in the ocean and help us to better understand its roles in regulating organic carbon flow and CO air–sea exchange.

MATERIALS AND METHODS

Study area. The estuary of the St. Lawrence River and the Gulf of St. Lawrence, referred to herein as the St. Lawrence estuarine system (SLES), is traditionally divided into 3 sections: the upper estuary extending from Quebec City to the mouth of the Saguenay Fjord, the lower estuary from the Saguenay Fjord to Pointe-des-Monts and the gulf east of Pointe-des-Monts (Fig. 1). With an area of 10 800 km^2 and a drainage basin of ~1.3 million km^2, the SLES receives the second largest freshwater discharge (600 km^3 yr^{-1}) in North America. Prominent hydrographic and oceanographic features of the SLES include runoff plumes from major tributaries (e.g. the Saguenay Fjord), upwelling near the head of lower estuary and a turbidity maximum zone (TMZ) slightly downstream from Île d'Orléans created by a complex density-driven circulation combined with the resuspension of bottom sediments (d'Anglejan & Smith 1973, Koutitonsky & Budgen

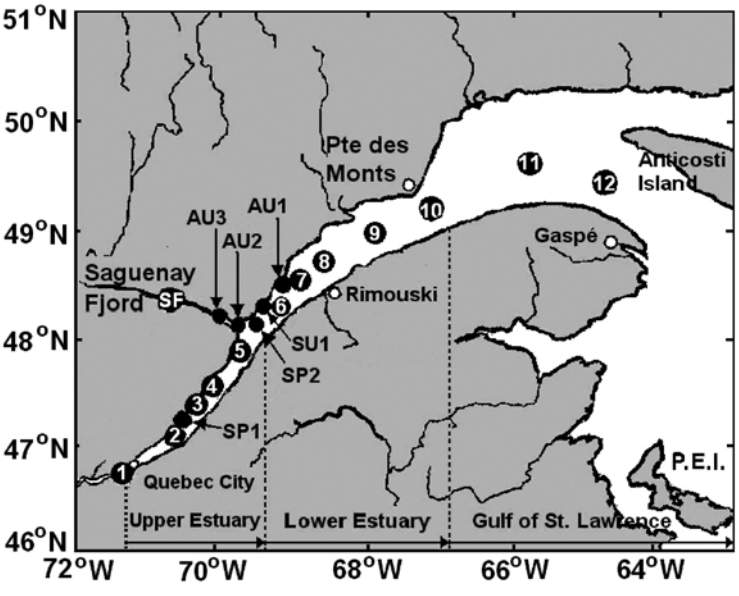

Fig. 1. Study area in the St. Lawrence estuarine system showing sampling stations 1 to 12 and spring-, summer- and autumn-only sampling stations (SP, SU and AU, respectively) SF: Saguenay Fjord station; P.E.I.: Prince Edward Island

1991). The water column is well mixed near the head of the estuary (Quebec City to slightly downstream from Île d'Orléans), but becomes partially mixed farther seaward and highly stratified in the lower estuary and the gulf (Painchaud & Therriault 1989, Gobeil 2006). Surface water transforms from freshwater-dominated case 2 water in the estuary to oceanic water-dominated case 1 water in the gulf (Nieke et al. 1997). The Saguenay Fjord is the SLES' principal tributary, where the water column is sharply stratified and the surface water is highly enriched with terrigenous dissolved organic matter. The production of phytoplankton in the upper estuary is suppressed by the instability and the high turbidity of the water column (Gobeil 2006). Primary productivity farther downstream is higher and typically peaks in spring in the gulf (Le Fouest et al. 2005) and in summer in the lower estuary (Therriault & Levasseur 1985). Nitrate usually becomes limiting after the phytoplankton blooms (Yeats 1988). Data concerning bacterial compartments in the SLES are rare. Some studies have demonstrated that bacterial dynamics in the upper estuary is controlled by both physical dispersion and bacterial production and predation (Lovejoy et al. 1993, Painchaud et al. 1995, 1996, Vincent et al. 1996). Attached bacteria constitute an important component of the total bacterial community in the upper estuary (Painchaud & Therriault 1989). Bacterial properties in the lower estuary and gulf remain obscure. Limited data show strong seasonal differences in bacterial activity in the gulf (Lovejoy et al. 1996, 2000).

Sampling. Sample collection was conducted in the SLES aboard the RV 'Coriolis II' in summer 2004 (24 to 31 July), autumn 2005 (30 September to 8 October) and spring 2007 (3 to 10 May). Sampling in early winter 2005 (15 to 18 December) was carried out aboard the Canadian Research Icebreaker CCGS 'Amundsen.' Sampling stations were distributed along a longitudinal transect from the upstream limit of the estuary near Quebec City to the gulf (Fig. 1). The summer and spring cruises also visited the Saguenay Fjord (Station [Stn] SF in Fig. 1), the principal tributary of the SLES with organic-rich surface waters. Two of the stations sampled in autumn only (Stns AU2 and AU3) were situated in the mouth of the Saguenay Fjord. A time-course station, Stn SP2, was occupied in spring to assess the effect of tide on K_{co}. Samples of surface waters (≤2 m depth) were taken in all seasons while deeper depths were sampled at certain localities in summer and spring only. Table 1 shows stations and depths sampled in each season.

Bulk water was taken with 12 l Niskin bottles mounted on a CTD rosette. A hand-held high-density polyethylene bucket was occasionally used to collect surface water. While being protected from light, water was immediately drawn into acid-cleaned 100 or 200 ml all-glass syringes fitted with 3-way nylon valves. The syringes were used for various CO incubations as delineated in the next section. CO blanks of the sampling bottles were checked by lowering them to 300 m at Stn 12, yielding 0.11 ± 0.04 nmol l^{-1} (mean ± SD) in summer and autumn, when no contamination-control measures were taken, and 0.05 ± 0.008 nmol l^{-1} in spring and winter, when the bottles were shielded from sunlight during transit between stations. These blanks were minor compared with the total [CO] at the start of each time-series incubation.

Chl *a* samples were collected onto 25 mm GF/F filters (Whatman). Suspended organic particles (SOP) were filtered onto pre-combusted and pre-weighted 47 mm GF/F glass fiber membranes (Millipore). The membranes were acidified with 10 ml of 10% v/v HCl to remove carbonates and rinsed with 10 ml of de-ionized water to remove salts. Samples for heterotrophic bacteria enumeration were transferred directly from the Niskin bottles into 5 ml sterile cryovials and fixed with glutaraldehyde (final concentration 0.1%). Chl *a*, SOP and bacterial samples were stored at −80°C for further analysis in a land-based laboratory.

Determination of K_{co}. Procedures for determination of the first-order rate constant, K_{co}, followed the whole water dark incubation method by Zafiriou et al. (2003) and Xie et al. (2005). Briefly, the 200 ml syringes containing the samples were incubated in the dark at the samples' *in situ* temperatures (±1°C) and analyzed for [CO] at appropriate times (usually 3 to 5 points per series). Each time series was fitted by an exponential, yielding K_{co}. In autumn and winter, when ambient [CO] was at times too low to construct time-decay series, small amounts of CO-enriched air were added to the incubation syringes, which were shaken for 3 min and the headspace gas removed. The amended samples' [CO] were <2 nmol l^{-1} in autumn and <1 nmol l^{-1} in winter; CO uptake followed first-order kinetics at these [CO]. Depending on CO consumption rates, incubation time varied from 1.5 to 37.5 h, within which bacterial abundance remains relatively stable (Painchaud et al. 1996). The method's precision was evaluated at Stns 7 and AU1 in autumn by incubating 5 replicates from each station, giving relative SD values of 8.3% (K_{co}: 1.33 ± 0.11 d^{-1}) and 7.1% (K_{co}: 1.69 ± 0.12 d^{-1}), respectively. The reproducibility of K_{co} measurement was occasionally checked with duplicate incubations, giving a mean difference between duplicates of 6 ± 2.8% (range: 4 to 11%, n = 5). It is assumed that errors for measurements without replicate incubations would be similar to those reported here. Note that this method measured net loss rate constants, which should be close to the corresponding gross loss rate constants since abiotic dark production of CO, based on the results of Zhang et al. (2008), was minor within CO turnover times obtained from this study.

Table 1. Microbial CO uptake rate constant (K_{co}) and the corresponding incubation temperature (IT), salinity, chlorophyll *a* concentration ([chl *a*]), concentration of suspended organic particles ([SOP]) and free-living bacterial abundance ($[BC]_f$) in the St. Lawrence River estuary and Gulf of St. Lawrence. Incubation temperatures were within ±1°C of *in situ* temperatures. nd: not determined; SF: Saguenay Fjord station; SU, AU and SP: summer-only, autumn-only and spring-only sampling stations, respectively

Stn	Depth (m)	IT (°C)	Salinity	[Chl *a*] (µg l^{-1})	[SOP] (mg l^{-1})	$[BC]_f$ (10^5 cells ml^{-1})	K_{co} (d^{-1})
Summer 2004							
1	2.0	22.0	0.11	21.08	5.80	5.53	12.58
3	2.0	20.0	5.47	9.49	8.10	4.69	5.54
5	2.1	15.0	19.32	1.21	3.10	3.11	4.08
6	2.0	15.0	26.20	15.25	1.03	4.89	6.62
	4.7	7.2	27.24	nd	nd	nd	3.10
7	0	15.0	25.79	19.41	1.28		10.56
9	2.0	15.0	24.17	23.01	1.44	6.54	14.38
10	2.1	15.0	28.52	8.43	0.63	nd	3.26
11	0	15.0	29.38	4.46	0.63	3.82	3.12
Surface water mean ± SD		16.5 ± 2.8	19.87 ± 11.06	12.79 ± 8.07	2.75 ± 2.77	4.77 ± 1.21	7.52 ± 4.40
2	1.5	22.0	1.61	20.43	46.78	5.79	14.78
12	2.2	15.0	28.66	6.54	0.82	3.33	1.78
	20.0	2.0	31.55	2.41	1.17	nd	1.28
SF	1.1	20.0	5.42	nd	nd	6.10	14.69
SU1	2.1	6.5	28.46	nd	nd	2.88	1.62
	22.5	2.0	30.76	nd	nd	nd	0.91
Autumn 2005							
1	2.0	17.1	0.01	0.20	7.92	16.03	12.34
3	2.0	13.1	9.00	0.37	9.93	7.42	6.41
4	2.0	6.5	23.55	0.02	6.64	6.18	2.47
5	0	7.0	24.17	0.42	2.62	6.25	2.81
6	0	5.7	26.07	0.36	1.42	5.60	2.22
7	2.0	3.5	29.50	0.20	1.19	5.35	1.31
8	2.0	6.7	26.45	0.42	1.15	6.87	3.00
9	2.0	6.7	29.33	1.27	1.15	15.83	3.36
10	2.0	7.0	27.81	1.05	1.10	11.29	3.22
Surface water mean ± SD		8.1 ± 4.2	21.76 ± 10.24	0.48 ± 0.41	3.68 ± 3.49	8.98 ± 4.31	4.12 ± 3.38
2	2.0	13.1	0.02	0.50	77.46	8.62	17.52
12	2.0	6.7	31.05	1.44	0.81	6.94	0.86
AU1	1.0	5.2	27.33	0.34	nd	nd	1.69
AU2	1.0	8.2	20.13	0.57	nd	nd	5.06
AU3	1.0	9.7	15.10	0.42	nd	nd	4.49
Winter 2006							
1	2.0	0.0	0.10	0.89	6.46	10.48	3.19
3	2.0	0.0	12.00	0.24	15.07	9.85	1.26
4	2.0	0.0	19.30	0.23	20.58	6.61	0.99
6	2.0	0.0	28.76	0.00	1.63	4.20	0.58
7	2.0	0.0	26.90	0.00	1.58	3.68	0.78
8	2.0	0.0	27.24	0.00	1.77	3.45	0.74
9	2.0	0.0	27.88	0.12	1.12	3.82	0.66
10	2.0	0.0	29.12	0.18	0.97	3.83	0.99
11	2.0	0.0	30.95	nd	nd	nd	0.60
Surface water mean ± SD		0.0 ± 0.0	22.47 ± 10.29	0.21 ± 0.29	6.15 ± 7.56	5.74 ± 2.91	1.09 ± 0.82
2	2.0	0.0	6.00	0.73	114.44	10.66	7.10
12	2.0	0.0	31.48	0.42	0.56	4.10	0.74
Spring 2007							
1	2.0	9.5	0.10	2.43	13.17	28.29	18.43
3	2.0	7.0	12.88	1.96	26.45	8.57	4.97
4	2.0	4.0	18.82	0.51	9.59	7.39	1.30
	10.0	2.0	24.56	nd	nd	5.24	1.74
	20.0	2.0	26.84	0.55	17.26	2.46	2.03
5	2.0	4.0	18.77	0.18	11.46	7.44	1.72
6	2.0	3.0	24.93	7.59	7.45	4.61	2.98
7	2.0	3.0	25.49	5.49	6.35	5.23	3.79
	10.0	1.0	27.50	nd	nd	5.13	1.30
	20.0	1.0	29.19	0.79	7.55	3.72	1.05
8	2.0	3.0	25.22	3.18	8.32	5.26	3.29
9	2.0	5.4	26.39	9.04	8.73	11.43	4.75

Table 1 (continued)

Stn	Depth (m)	IT (°C)	Salinity	[Chl *a*] (µg l^{-1})	[SOP] (mg l^{-1})	$[BC]_f$ (10^5 cells ml^{-1})	K_{co} (d^{-1})
Surface water mean ± SD		4.9 ± 2.3	19.07 ± 8.99	3.80 ± 3.26	11.44 ± 6.44	9.78 ± 7.80	5.15 ± 5.52
2	2.0	7.0	0.73	10.10	116.18	17.34	39.84
12	2.0	2.0	31.64	38.32	9.00	13.13	0th order
	10.0	1.0	31.67	nd	nd	12.64	0th order
	20.0	1.0	31.89	5.00	4.27	6.14	0.81
SF	2.0	4.0	4.12	1.62	4.71	8.82	0th order
	10.0	2.0	24.70	nd	nd	7.07	1.90
	20.0	2.0	27.50	nd	nd	3.26	1.25
SP1	2.0	5.8	13.54	nd	nd	8.14	3.84
SP2 (low tide)	2.0	2.0	25.40	0.94	8.77	3.94	1.30
SP2 (high tide)	2.0	2.0	30.40	0.75	6.98	3.47	0.93
SP2 (intertide)	2.0	2.0	28.15	0.88	6.21	3.59	1.00

***T*-dependence and Michaelis-Menten kinetics studies.** Incubations for studying the *T*-effect on K_{co} were conducted in summer at Stns 1, 2, 3, 7, 9, 11, SF and SU1. The 200 ml syringes containing the samples were incubated in the dark at 3 temperatures, including the one at the sample's *in situ* temperature. Procedures for K_{co} determination are described in the previous section. The K_{co} data for each station were fitted to the linearized Arrhenius equation to derive the activation energy, E_a.

Approaches for the Michaelis-Menten kinetics study were modified from Xie et al. (2005, 2009). From 7 to 14 replicate incubation syringes (100 ml each) were amended with CO-free or CO-enriched air and shaken for 3 min. The headspace gas was then expelled, yielding 7 to 14 different initial [CO]. Each syringe was analyzed for [CO] close to the time of preparation, incubated in the dark and analyzed a second time. Incubation durations were optimized to produce measurable rates of CO consumption while changes in [CO] were minimal. CO uptake rates (v) in all syringes were pooled together and V_{max} and K_m were derived from nonlinear fitting (v versus [CO]) of the Michaelis-Menten equation, $v = V_{max}[CO]([CO] + K_m)^{-1}$ and from linear fitting ([CO] v^{-1} versus [CO]) of the Hanes plot, $[CO]\ v^{-1} = [CO]\ V_{max}^{-1} + K_m\ V_{max}^{-1}$. The Hanes plot is preferred over other linearized Michaelis-Menten forms to compute V_{max} and K_m (Cornish-Bowden 1995). We employed the Michaelis-Menten kinetic model for whole community uptake of CO, and we recognize that this model was originally developed for a single enzyme system but was later adapted for natural microbial communities (Wright & Hobbie 1965).

Analysis. Incubation syringes were subsampled using 50 ml glass syringes fitted with 3-way nylon valves; the latter were flushed twice with sample water before the final filling. [CO] was measured using a manual headspace method (Xie et al. 2002). Briefly, 5 ml CO-free air was introduced into the sample-filled 50 ml syringes (a gas:water ratio of 1:6). The syringe was vigorously shaken for 3 min and the equilibrated headspace air was injected into a modified Trace Analytical TA3000 reduction gas analyzer for CO quantification. The system was standardized by frequent injections of a gaseous CO standard (1.23 ppm, Praxair) using a wetted 10 ml glass syringe (100% relative humidity). Precision of the [CO] measurement was estimated to be ±0.02 nmol l^{-1} (or ±2%).

Filters retaining SOP were lyophilized and the concentration of SOP, [SOP], was determined by weight difference corrected for the volume of the filtered water. Measurement of [chl *a*] followed the HPLC method by Zapata et al. (2000). Free-living bacterial abundance, $[BC]_f$, was determined using an Epics Altra flow cytometer (Beckman Coulter) equipped with a 488 nm argon laser operated at 15 mW. A 0.5 ml subsample was half diluted in 1× Tris-EDTA buffer (pH 8) and the resulting 1 ml solution was incubated with 0.25 µl SYBR Green I (Ci = 10 000×, Invitrogen) for 30 min at room temperature in the dark. We added 10 ml fluorescent beads (1 µm in diameter; Fluoresbrite Plain, YG) to each sample as an internal standard and then analyzed the samples with the cytometer for 3 min. $[BC]_f$ was calculated from the analysis volume that had been gravimetrically determined and corrected for the dead volume (50 µl, i.e. the volume taken from the sample tube but not accounted for when data acquisition was stopped). Salinity (S) was determined with a salinometer (model 8410A, Portasal).

RESULTS

Spatial and seasonal variation of K_{co}

Microbial CO uptake in the SLES approximated first-order kinetics in most cases. Fig. 2 shows typical first-order CO decay curves and Table 1 compiles K_{co}

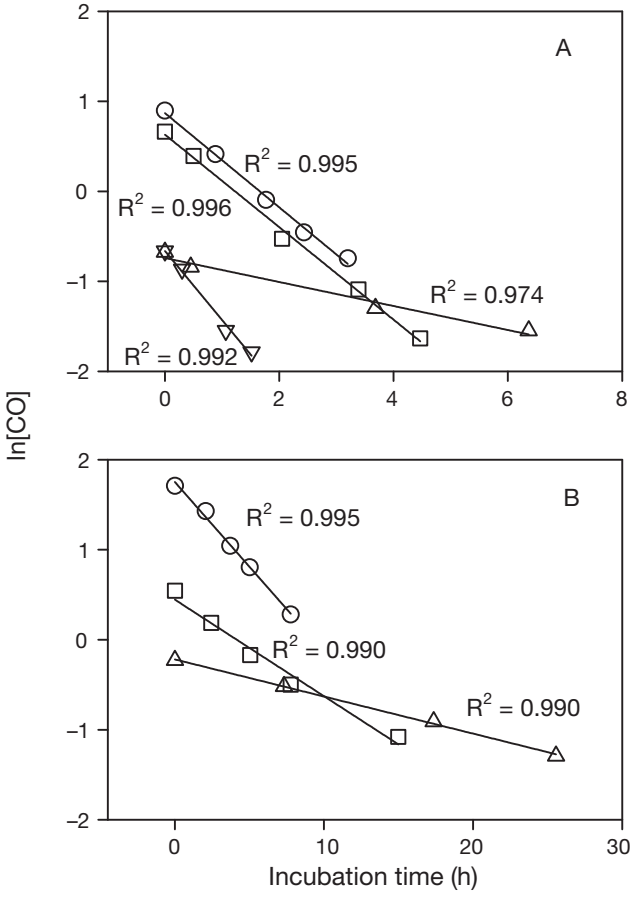

Fig. 2. Typical ln[CO] versus incubation time plots showing first-order CO uptake kinetics at (A) Stn 1 and (B) Stn 10 in summer (○), autumn (□), winter (△) and spring (▽). Stn 10 was not sampled in spring. Sampling depths were 2 m for both stations. Lines are the best fits of the data. R^2 is correlation coefficient of determination

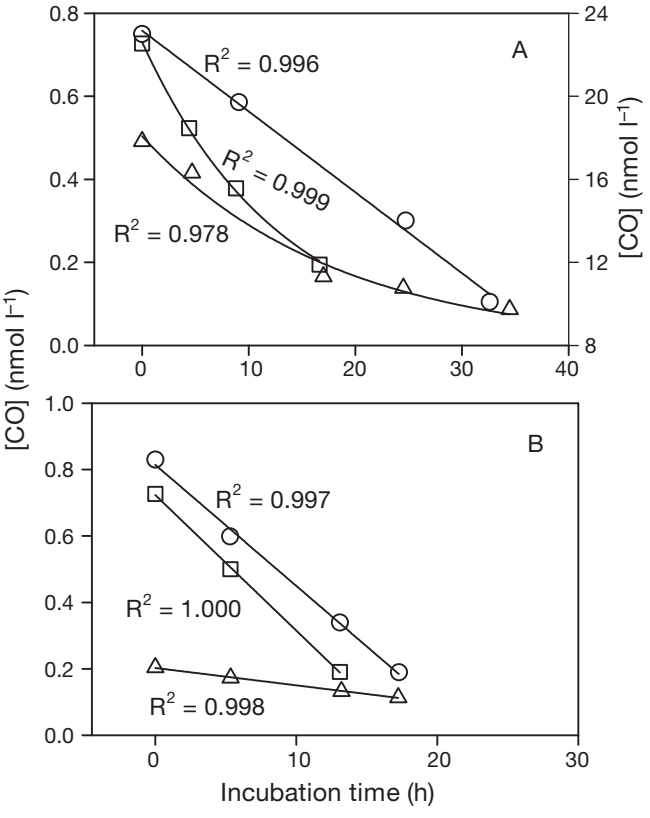

Fig. 3. [CO] versus incubation time plots showing saturation (straight lines) and first-order (curved lines) kinetics of CO uptake at (A) Stn SF (Saguenay Fjord) and (B) Stn 12 for 3 depths: 2 m (○), 10 m (□) and 20 m (△). [CO] at 2 m in (A) is on the right *y*-axis scale. Lines are the best fit plots of the data

data and other related variables. At the surface (<2.5 m) the upper estuary showed the highest K_{co} in all seasons (8.48 ± 4.16 d^{-1} [mean ± SD]) followed by the lower estuary (3.94 ± 3.40 d^{-1}) and the gulf area (1.32 ± 0.98 d^{-1}). The largest K_{co} among individual stations always occurred at Stn 2 located in the TMZ (see [SOP] in Table 1), suggesting that attached bacteria played an important role in CO uptake there. K_{co} decreased vertically with depth at Stns 6 and 12 in summer and Stn 7 in spring, in line with the distributions of *T* and $[BC]_f$ (Table 1). The K_{co} depth distribution, however, reversed at Stn 4 in spring at which *T* and $[BC]_f$ decreased with depth but [SOP] at 20 m nearly doubled that at 2 m (Table 1), again implying enhancement of CO consumption by attached bacteria. Stn SP2 in spring revealed a clear tidal effect on K_{co}: high at low tide (1.30 d^{-1}), low at high tide (0.93 d^{-1}) and intermediate at intertide (1.00 d^{-1}), showing an inverse trend with salinity (Table 1). In spring, Stn SF displayed saturation (zero-order) kinetics at 2 m, where *in situ* [CO] reached >20 nmol l^{-1}, and switched to first-order kinetics at deeper depths (10 and 20 m), where *in situ* [CO] dropped to <1 nmol l^{-1} (Fig. 3A). Stn 12, however, exhibited saturation kinetics at all 3 sampled depths (2, 10 and 20 m) despite low *in situ* [CO] (<1 nmol l^{-1}) (Fig. 3B).

Seasonally, surface water (<2.5 m) K_{co} decreased in descending order from its highest value in summer (7.52 ± 4.40 d^{-1}) followed by spring (5.15 ± 5.52 d^{-1}) and autumn (4.12 ± 3.38 d^{-1}) to its lowest value in winter (1.09 ± 0.82 d^{-1}), a trend that mimicked the seasonal patterns of [chl *a*] (not proportionally) and water *T* (except in spring) but not $[BC]_f$ (Table 1). Stns 2 and 12 were excluded from this comparison as in spring Stn 2 biases the mean K_{co} to be unusually high (5.51 versus 9.01 d^{-1}) and Stn 12 did not abide by the first-order kinetics (Table 1). The seasonality of K_{co} at Stn 2 was strongly linked to that of [SOP]: high [SOP] in spring and winter corresponded to relatively high K_{co} values compared with summer when [SOP] was much lower (Table 1). This linkage is more clearly indicated by the positive correlation between the ratio K_{co} (Stn 2):K_{co}

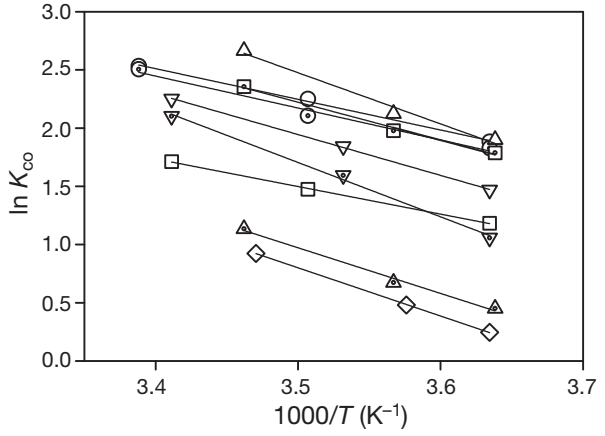

Fig. 4. Arrhenius plots of first-order CO uptake rate constant (K_{co}) for Stns 1 (○), 2 (⊙), 3 (□), 7(⊡), 9 (△), 11 (◬), SF at 2 m (▽), SF at 9 m (▼) and SU1 (◇). Lines are the best fit plots of the data. Coefficients of determination (R^2) and activation energies derived from these plots are shown in Table 2. T: temperature; see Table 1 for station abbreviations

(Stn 1) and [SOP] at Stn 2 (R^2 = 0.957, n = 4). Stn 1 was chosen as a reference as it was only slightly upstream of Stn 2 but had far less SOP (Table 1).

K_{co} in the SLES at winter's freezing water temperatures (1.05 d^{-1}) is comparable to K_{co} in the near-shore southeastern Beaufort Sea in autumn (0.98 d^{-1}) (Xie et al. 2005). The summer's K_{co} in the SLES (7.25 d^{-1}) is much smaller than K_{co} in the warmer and organically richer Delaware Bay (26.6 d^{-1}) but close to the value in the coastal northwest Atlantic Ocean (7.92 d^{-1}) (Xie et al. 2005). If compared over the same salinity range from 0 to 30, our surface water K_{co} values are similar to those in the more southern Yaquina Bay in Oregon (Butler et al. 1987) for summer (7.25 versus 7.37 d^{-1}), spring (5.15 versus 5.13 d^{-1}) and winter (1.05 versus 1.00 d^{-1}), but smaller for autumn (4.12 versus 6.79 d^{-1}). In view of the warmer water temperatures in Yaquina Bay (>10°C higher in winter and ≥5°C higher in the other 3 seasons), biotic and abiotic variables, in addition to T, that regulate CO consumption should differ considerably between the 2 systems. The difference in methodology also may have played a role. Butler et al. (1987) used the ^{14}C technique to determine K_{co} while we employed the whole water incubation method (see Xie et al. 2005).

Temperature-dependence of K_{co}

Summer's T-dependence incubations all showed linear Arrhenius plots (Fig. 4) with varying slopes and thereby E_a values (Table 2). E_a for the upper estuary (S: 0.11 to 5.47) is lower than for the lower estuary and gulf (S: 24.17 to 29.38): 21.5 ± 1.6 versus 32.7 ± 4.0 kJ mol^{-1}. The Saguenay Fjord's E_a values are higher than those for the estuary and gulf based on salinity. The deeper, saltier sample from the fjord, however, also gives a higher E_a value than does the less saline surface sample (Table 2). The Q_{10} values demonstrate that for a 10°C increase K_{co} rises on average by 40% in the low salinity samples (S < 6) and by 64% in the more saline samples (S: 14.84 to 29.38).

In summer the difference in T could cause K_{co} at Stn 1 (22°C) to be only 78% higher than K_{co} at Stn 12 (15°C), which is far below the observed discrepancy (12.58 versus 1.78 d^{-1}). Similarly, the expected T effects in autumn and spring could account for only small portions of the observed differences in K_{co} between the 2 stations if summer's E_a values are assumed. Hence, other variables, such as salinity, pH and nutrients, which, together with T, regulate bacterial abundance, composition and activity, should have been important in controlling CO consumption in these 3 seasons.

In winter little T effect on K_{co} is expected since T was nearly constant throughout the SLES. Furthermore, variations of pH in the SLES are small (7.76 to 8.10, Lebel & Pelletier 1980, Zhang et al. 2008) and nutrients should be relatively abundant in winter due to low primary production and strong vertical mixing. Consequently, salinity would be the dominant factor controlling microbial CO uptake as demonstrated by the strong inverse correlation of K_{co} to S (Table 3). Partial correlation analysis confirms that this relation largely stemmed from the inverse correlation of $[BC]_f$ to S (R^2 = 0.928, n = 10). Thus, physical dispersion of bacteria during estuarine mixing (Painchaud & Therriault 1989, 1995, 1996) played a central role in dictating the dynamics of K_{co} in winter.

Table 2. Activation energy (E_a) and Q_{10} obtained from temperature-dependent incubations in summer 2004. Q_{10} is defined as the ratio of K_{co} at 20°C to K_{co} at 10°C. R^2 is the coefficient of determination for the Arrhenius plots in Fig. 4. See Table 1 for station abbreviations

Stn	Depth (m)	Salinity	E_a (kJ mol^{-1})	Q_{10}	R^2
1	2	0.11	21.91	1.4	0.997
2	1.5	1.61	22.82	1.4	0.985
3	2	5.47	19.70	1.3	0.999
7	0	25.79	27.08	1.5	0.994
9	2	24.17	36.52	1.7	0.984
11	0	29.38	32.60	1.6	0.992
SU1	2	28.46	34.45	1.6	1.000
SF	2	4.70	29.14	1.5	1.000
SF	9	14.84	38.80	1.8	0.996

Michaelis-Menten kinetics

Results of Michaelis-Menten kinetics studies are summarized in Table 4 and examples of Michaelis-Menten plots are shown in Fig. 5. Nonlinear regression and linearized Hanes plots generally give similar values of K_m and V_{max}, the averages of the 2 methods being reported here. In autumn V_{max} spanned from 0.21 nmol l^{-1} h^{-1} in the saltiest sample (Stn 12) to 3.48 nmol l^{-1} h^{-1} in the least saline sample (Stn 1). V_{max} negatively correlates with salinity: $V_{max} = -0.086\ S + 2.81$ ($R^2 = 0.772$, n = 8). In winter V_{max} of 0.91 nmol l^{-1} h^{-1} in the freshest sample (Stn 1) was ca. 6 times the mean V_{max} of 0.16 nmol l^{-1} h^{-1} in the remaining samples whose salinity fell in a narrow range of 27.24 to 31.48. Autumn K_m values ranged from 1.34 to 5.91 nmol l^{-1} [CO] (mean: 3.24 nmol l^{-1} [CO]) and showed no consistent trend with salinity. Winter K_m values ranged from 1.84 to 9.18 nmol l^{-1} [CO] (mean: 4.87 nmol l^{-1} [CO]) and its variation did not correspond to salinity either. Saturation of CO uptake occurred at 5 to 10 nmol l^{-1} [CO], depending on locations. Inhibition of CO uptake was observed at Stns 4, 12 and AU1 in autumn at [CO] greater than 14.5, 21.2, and 20.6 nmol l^{-1}, respectively, and at Stn 12 in winter at [CO] > 16.7 nmol l^{-1}. For other stations the amended upper bound [CO], 10.7 to 20.2 nmol l^{-1} in autumn and 12.0 to 18.1 nmol l^{-1} in winter, were not sufficiently high to detect inhibition behavior.

Table 3. Results of regression analysis between microbial CO uptake rate constant (K_{co} in d^{-1}) and various abiotic and biotic variables. Salinity (S) is expressed without units, temperature (T) is in Kelvin, chlorophyll *a* concentration ([chl *a*]) is in µg l^{-1}, free bacterial abundance ($[BC]_f$) is in cells ml^{-1}, and suspended organic particles ([SOP]) are in mg l^{-1}. A and Y_0 are fitted parameters and stand for the proportionality constant and the intercept, respectively. Stn 2 is removed for data fitting except for summer. R^2 is the coefficient of determination of predicted K_{co} versus measured K_{co}

	A	Y_0	R^2	n
$K_{co} = A \times S + Y_0$				
Summer	−0.29	12.21	0.456	18
Autumn	−0.304	10.59	0.872	13
Winter	−0.07	2.70	0.831	10
Spring	−0.44	13.24	0.680	18
4 seasons	−0.31	10.74	0.505	59
$K_{co} = A \times T + Y_0$				
Summer	0.56	−154.05	0.52	18
Autumn	0.78	−217.02	0.897	13
Spring	1.49	−408.54	0.696	18
3 seasons	0.50	−134.89	0.534	49
$K_{co} = A \times$ [chl *a*] $+ Y_0$				
Summer	0.59	0.065	0.871	11
Autumn	−1.91	4.85	0.0772	13
Winter	2.54	0.52	0.800	9
Spring	0.31	2.84	0.0376	13
4 seasons	0.45	2.30	0.442	46
$K_{co} = A \times [BC]_f + Y_0$				
Summer	3.45×10^{-5}	−7.60	0.744	11
Autumn	5.26×10^{-6}	−0.82	0.418	10
Winter	2.34×10^{-6}	0.194	0.641	9
Spring	6.61×10^{-6}	−1.37	0.913	18
4 seasons	5.07×10^{-6}	0.75	0.251	48
$K_{co} = A \times$ [SOP] $+ Y_0$				
Summer	0.20	5.81	0.284	11
Autumn	0.69	1.46	0.495	10
Winter	0.025	0.97	0.0514	9
Spring	0.21	1.37	0.0682	13
4 seasons	0.18	2.83	0.120	43
$\ln K_{co} = \ln[BC]_f + A \times T^{-1} + Y_0$				
Summer	−8259.1	17.32	0.728	11
Autumn	−8173.7	16.55	0.903	10
Spring	−7513.8	14.67	0.949	19
4 seasons	−8439.3	17.84	0.770	49
$\ln K_{co} = \ln$[chl *a*] $+ A \times T^{-1} + Y_0$				
Summer	−591.4	1.57	0.882	11
Autumn	−14617.3	54.09	0.202	13
Spring	−17937.6	65.18	0.381	14
4 seasons	7320.8	−25.00	0.150	47

DISCUSSION

Predictive tools for K_{co}

Results of regression analysis between K_{co} and various variables are displayed in Table 3. Excluding Stn 2 (excepting summer), K_{co} exhibits significant ($p < 0.05$), negative correlations with S in autumn, winter and spring, and positive correlations with T in autumn and spring, [chl *a*] in summer and winter, and $[BC]_f$ in summer, winter and spring. In spring, however, the correlation between K_{co} and S or $[BC]_f$ is unduly influenced by Stn 1; eliminating it greatly reduces the degree of correlation with $[BC]_f$ ($R^2 = 0.456$) and nulls the relationship with S. The same is true for the correlation of K_{co} with [chl *a*] in winter. A weakly significant correlation between K_{co} and [SOP] exists only in autumn if Stn 2 is omitted; including Stn 2, nonetheless, leads to significant correlations (R^2: 0.716 to 0.858) for all seasons except summer, demonstrating an excessive weight by Stn 2 in seasons other than summer. Pooling data from all seasons yields weak but significant ($p < 0.05$) correlations of K_{co} to S, T, or [chl *a*] but not to $[BC]_f$ or [SOP].

Multivariable regression analyses were performed between K_{co} and T and $[BC]_f$ or between K_{co} and T and

Table 4. Results of regression analysis of the Michaelis-Menten kinetics model for microbial CO consumption by nonlinear fitting or the linearized Hanes plot. V_{max} = maximum CO consumption rate; K_m = [CO] at $V_{max}/2$. IT: incubation temperature; a^0_s: CO specific affinity; nd: not determined; AU: autumn-only sampling station

Stn	IT (°C)	Salinity	K_m (nmol l^{-1})		V_{max} (nmol l^{-1} h^{-1})		a^0_s	R^2		n
			Nonlinear	Hanes	Nonlinear	Hanes	(l (mg of cell)$^{-1}$ h^{-1})	Nonlinear	Hanes	
Autumn										
1	17.1	0.12	3.74	3.70	3.58	3.37	2.33	0.914	0.924	9
3	13.1	7.75	6.46	5.36	1.32	1.21	1.16	0.954	0.201	9
4	6.5	23.24	1.87	2.50	0.32	0.32	0.97	0.873	0.926	9
6	5.7	26.07	3.52	4.13	1.29	1.25	2.39	0.952	0.938	14
7	3.5	29.44	3.82	3.31	0.25	0.23	0.50	0.833	0.920	8
10	7	27.68	1.37	1.32	0.42	0.36	1.03	0.757	0.900	10
12	6.7	31.02	3.06	3.01	0.22	0.20	0.40	0.708	0.838	11
AU1	5.2	27.33	2.14	2.46	0.38	0.38	nd	0.928	0.970	7
Winter										
1	0	0.1	3.43	4.48	0.88	0.94	0.89	0.939	0.891	11
6	0	28.76	2.20	1.48	0.11	0.09	0.53	0.799	0.893	9
8	0	27.24	2.76	3.66	0.16	0.16	0.59	0.897	0.882	8
9	0	27.88	9.40	7.47	0.23	0.20	0.27	0.901	0.793	8
10	0	29.12	2.45	2.75	0.14	0.14	0.56	0.931	0.947	9
12	0	31.48	10.71	7.65	0.21	0.17	0.20	0.935	0.736	9

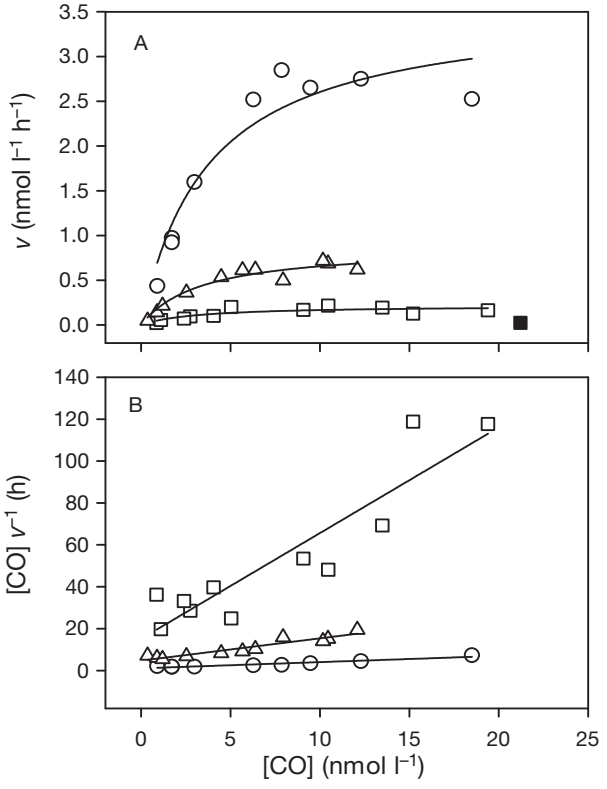

Fig. 5. Examples of nonlinear (A) Michaelis-Menten plots and (B) the corresponding linear Hanes plots for Stn 1 in autumn (○), Stn 12 in autumn (□) and Stn 1 in winter (△). Lines in (A) are nonlinear least-square fits of data using the equation: $v = V_{max}$ [CO] ([CO] + K_m)$^{-1}$, where v is the CO uptake rate. The filled square for Stn 12 shows inhibition of CO uptake and is excluded from data fitting. Lines in (B) are best linear fits of the data. See Table 4 for definitions and results of regression analyses

[chl *a*], assuming that the *T*-dependence of K_{co} followed the Arrhenius behavior and that K_{co} was proportional to $[BC]_f$ or [chl *a*] (Table 3). The K_{co}–*T*–$[BC]_f$ relationships are significant ($p < 0.05$) for summer, autumn and spring, while the K_{co}–*T*–[chl *a*] relationships are significant only in summer (analysis was not performed for winter since *T* in winter was nearly constant). Pooling data from all 4 seasons gives a significant correlation of K_{co} to *T* and $[BC]_f$ but not to *T* and [chl *a*] (Table 3). Fig. 6 compares K_{co} values predicted from *T* and $[BC]_f$ with the measured ones. *T* and $[BC]_f$ account for 77% of the K_{co} variance while *T* and [chl *a*] only account for 15% (Table 3).

Based on the above regression analyses, S is a statistically valid indicator of K_{co} in autumn and winter, *T* in autumn and spring, [chl *a*] in summer and $[BC]_f$ in summer and winter. The combination of $[BC]_f$ and *T* emerges as the only all-season indicator of K_{co}. However, unlike [chl *a*], which can often be retrieved via remote sensing, $[BC]_f$ is more difficult to acquire on large temporal and spatial scales, thereby limiting its potential as a predictive tool for K_{co}.

Effect of suspended particles on microbial CO uptake

The highly enhanced microbial CO uptake at Stn 2 in autumn, winter and spring should have resulted from CO consumption by bacteria attached on suspended particles. Particle-based CO uptake could also exist at other stations, though to a lesser extent because of lower particle loads. Painchaud & Therri-

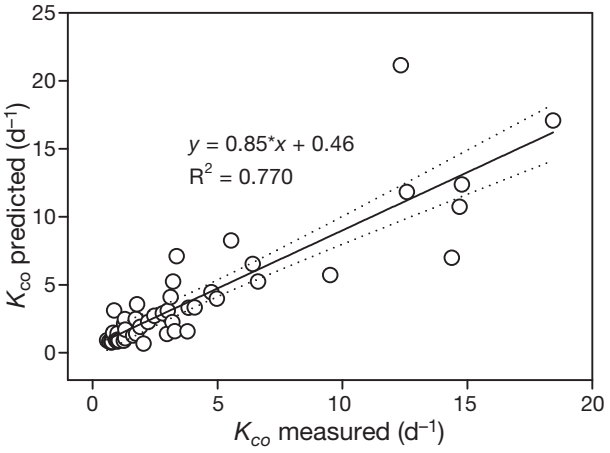

Fig. 6. First-order CO uptake rate constants (K_{co}) predicted from the equation: $\ln K_{co} = \ln[BC] + A \times T^{-1} + Y_0$ (Table 3) versus measured K_{co} values for all-season data. Solid line is the best fit plot of the data and broken lines are 95% confidence intervals. Data from Stn 2 in the turbidity maximum zone are excluded for autumn, winter and spring

ault (1989) have reported that attached bacteria in the upper St. Lawrence River estuary in summer are linearly correlated to particulate organic carbon and occupy important fractions of the total bacteria populations: 14 to 30% (23 ± 6%) in the 0 to 10 m layer and 17 to 64% (34 ± 16%) in the 10 m bottom layer, with the largest values observed in the TMZ. The fractions and absolute values could be greater, particularly in and adjacent to the TMZ, in spring, autumn and winter when particle loads are higher than in summer (Table 1). Directly quantifying the effect of particles on CO uptake is not possible as attached bacterial abundance, $[BC]_a$, was not determined. However, we indirectly evaluated this effect by assuming $[BC]_a = f_p \times [BC]_f \times [SOP]$, where f_p is a season-specific proportionality constant, representing the fraction of free bacterial cells attached on the particles per unit of [SOP]. The total bacterial abundance, $[BC]_t$, in a whole water sample is then expressed as $[BC]_t = (1 + f_p \times [SOP]) \times [BC]_f$. An arbitrary value of f_p is assigned and $[BC]_t$ calculated. K_{co} is then fitted to the equation $\ln K_{co} = \ln[BC]_t + A \times T^{-1}$, where A is a constant. Note that this equation does not contain the constant (Y_0) term since statistical results indicate that A and Y_0 are highly dependent. The optimum value of f_p is determined iteratively by minimizing the sum of squares of the differences between the measured K_{co} and the K_{co} predicted from this model. Fig. 7 indicates that the proposed model well explains the enhanced CO uptake at Stn 2 and greatly improves the overall performance of data fitting for autumn, winter, spring and all 4 seasons combined, but not for summer (data not shown) when particle loads are much lower. Based on

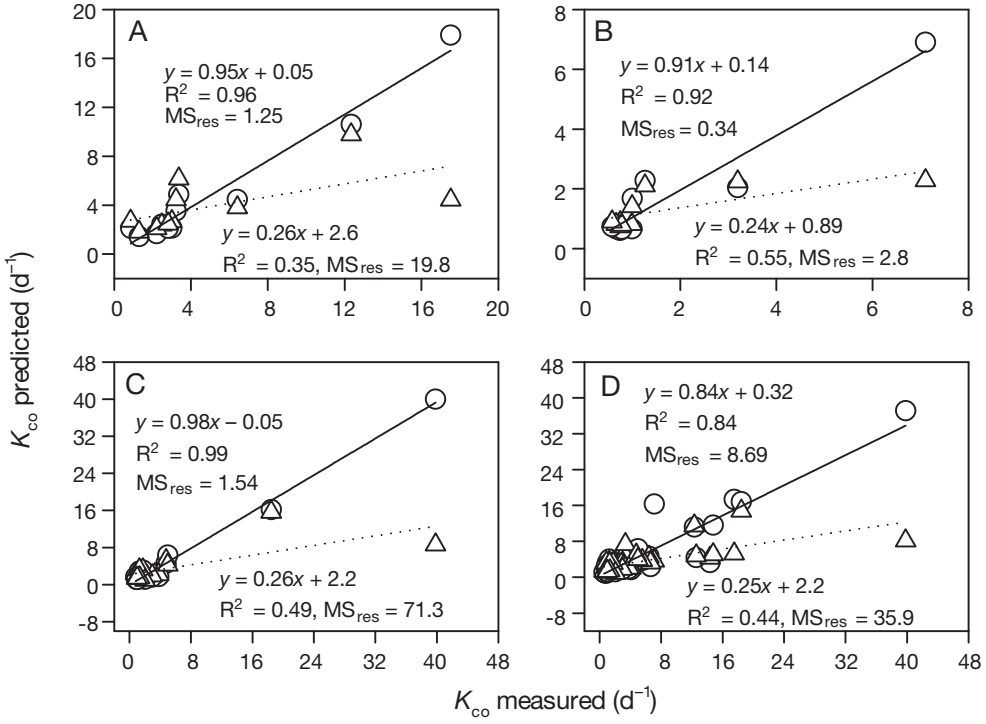

Fig. 7. First-order CO uptake rate constants (K_{co}) predicted from the equation $\ln K_{co} = \ln[BC] + A \times T^{-1}$ versus measured K_{co} values after (○ and solid lines) and before (△ and dotted lines) taking into the particle effect for (A) autumn, (B) winter, (C) spring, and (D) all 4 seasons combined. Data are from all stations, including Stn 2 in the turbidity maximum zone. Lines are the best fits of the data. MS_{res} is the residual mean square

the f_p value, the particle effect is the strongest in spring (f_p = 0.062 l mg^{-1}) followed by autumn (f_p = 0.057 l mg^{-1}), winter (f_p = 0.025 l mg^{-1}) and summer (f_p = 0.013 l mg^{-1}). The present study, therefore, indirectly proves an important role of particle load and its seasonality in regulating microbial CO uptake in particle-rich waters. It should be pointed out that this model does not intend to propose mechanisms of ecological interactions between free-living and attached bacteria. Rather, it mainly aims at providing an empirical quantitative formula to assess the effect of suspended particles on microbial CO consumption.

Implications of CO uptake kinetics

Xie et al. (2009) reported saturation and inhibition of microbial CO uptake at elevated ambient [CO] in surface waters of the Arctic Ocean in spring. The present study detected saturation kinetics in the top layer at Stn SF again in spring (Fig. 3A; water T = 4°C; [CO] = 23.0 nmol l^{-1}), but not during the warmer summertime (water T = 20°C; [CO] = 0.82 nmol l^{-1}) (Table 1). Saturation or inhibition at high ambient [CO] may, therefore, be common in cold waters during vernal warming when increasing solar irradiances result in an elevated CO production but relatively low water temperatures depress bacterial activity. The more surprising observation in the present study is the saturation of CO uptake at very low *in situ* [CO] (<0.83 nmol l^{-1}) occurring from the surface down to 20 m at Stn 12 in spring (Fig. 3B). This could arise from the presence of microbes with exceptionally high-affinity CO uptake systems or with unusual CO-uptake physiology at this particular locality and time. Further investigations are needed to clarify this issue.

Uptake of certain organic substrates by natural microbial assemblages follows multiphasic kinetics and is enhanced with decreasing substrate concentrations (Azam & Hodson 1981, Lewis et al. 1988). A single pair of K_m and V_{max} values thus cannot adequately describe this behavior since K_m, V_{max}, and their ratio change with substrate concentrations (e.g. Lewis et al. 1988). Based on theory as related to cytoarchitecture, Button and co-workers (e.g. Button 1998, Button et al. 2004) developed the concept of specific affinity (a^0_s) to supersede the Michaelis-Menten model: a^0_s is defined as the bacterial biomass-normalized uptake rate constant at near-zero substrate concentration.

The present study did not detect multiphasic kinetics for microbial CO uptake, which is consistent with previous studies (Tolli & Taylor 2005, Xie et al. 2005, 2009). As the upper bounds of [CO] tested are well beyond the ambient [CO] in the SLES and in most marine waters, multiphasic kinetics is generally not expected for CO uptake in natural waters. On the contrary, all CO uptake data from the present study exhibited single-phase, hyperbolic, Michaelis-Menten kinetics until inhibition is reached at sufficiently high [CO]. K_m and V_{max} are thus appropriate parameters to characterize the CO uptake process. K_m values, including those from past studies, seldom exceed 10 nmol l^{-1} [CO] and mostly are below 6 nmol l^{-1} [CO], revealing high-affinity CO uptake systems. Diverse taxonomic bacteria are capable of oxidizing CO despite the elusiveness of their species-level identities (Tolli et al. 2006, King & Weber 2007, Moran & Miller 2007). The narrow range of K_m thus implies that only a few species dominate CO uptake or a diversity of species possess uptake systems with similar CO affinities.

Xie et al. (2009) observed Hill-type (sigmoidal) CO uptake kinetics with threshold [CO] in nutrient-depleted surface waters of the Arctic Ocean in spring. However, these kinetic characteristics were not observed in warmer and/or nutrient-richer waters in the SLES (present study, autumn and winter), the northwest Atlantic Ocean (summer), and the coastal Arctic Ocean (autumn) (Xie et al. 2005). In the SLES the low CO uptake activation energies of <40 kJ mol^{-1} (Table 2) conform to the activation energy of ~40 kJ mol^{-1} found for nutrient-sufficient microbial growth (Felip et al. 1996). According to the cytoarchitecture-based theory (Button 1998, Button et al. 2004), Hill-type curves and threshold substrate concentrations are related to energy requirements for building cell membrane potentials to prime active substrate transport, which are particularly relevant to microorganisms in low-energy (i.e. cold) and low-nutrient environments during spring warming. Warm and nutrient-rich conditions act to maintain energized cell membranes and thereby reduce or eliminate threshold substrate concentrations and Hill-type curvature (Button 1998, Button et al. 2004). Results from this and previous field studies are, therefore, consistent with the predictions by Button et al. (2004).

For comparison with processes of microbial uptake of organic substrates, a^0_s values of CO uptake are calculated as the V_{max}:K_m ratio divided by bacterial biomass (Button et al. 2004). Carbon-based bacterial biomass is estimated from $[BC]_f$ by using a conversion factor of 25 fg C cell^{-1} (Bell 1993) and converted to wet cell biomass according to Button (1998). The wet cell biomass-based a^0_s values are included in Table 4. The mean a^0_s in autumn (1.25 ± 0.80 l (mg of cell)$^{-1}$ h^{-1}) is more than double that in winter (0.51 ± 0.25 l mg of cell)$^{-1}$ h^{-1}), which in part should be attributed to warmer temperatures in autumn and is consistent with findings for microbial uptake of organic substrates (Button et al. 2004). Intraseasonally high a^0_s values

usually correspond to low salinities in both seasons and to high temperatures in autumn (with the exception of Stn 6). These CO a^0_s values lie in the upper bounds of the a^0_s values for various organic substrates in the literature, which vary over several orders of magnitude (Button 1998, Button et al. 2004).

CONCLUSIONS

CO uptake generally followed first-order kinetics throughout the SLES and in all 4 seasons with the exception of 2 localities (Stns SF and 12) where saturation kinetics occurred in spring. In all seasons the first-order CO uptake rate constant, K_{co}, decreased from the upper estuary to the lower estuary to the Gulf. K_{co} displayed a large seasonality, decreasing in order from its highest value in summer followed by spring and autumn to its lowest value in winter, and tide-dependence, in decreasing order of low tide > inter-tide > high tide. Particle-associated microbes accelerated CO uptake, resulting in the fastest consumption to occur in the TMZ. Microbes in high saline waters exhibited stronger *T*-dependence of CO uptake than the low saline counterparts. Salinity, *T*, [chl *a*], and $[BC]_f$ can be used as a proxy of K_{co} in, respectively, autumn and winter, autumn and spring, summer, and summer and winter. The combination of $[BC]_f$ and *T* can be used as an all-season predictive tool for K_{co}. Microbial CO uptake followed single-phase Michaelis-Menten kinetics with K_m falling in a narrow range of low-nanomolar concentrations. CO specific affinities are within the ranges of those for various organic substrates. The present study demonstrates substantial seasonal variations in microbial CO uptake and complex influences of various biotic and abiotic variables on this process.

Acknowledgements. T. Lou assisted in sample collection and analysis during the summer cruise. We thank the chief scientists, colleagues, captains and crews of the RV 'Coriolis II' and CCGS 'Amundsen' cruises. This work was supported by grants to H.X. from the Natural Sciences and Engineering Research Council of Canada (NSERC) and the Canada Foundation for Innovation (CFI). This is a contribution to the research programs of the Institut des sciences de la mer de Rimouski (ISMER).

LITERATURE CITED

Azam F, Hodson RE (1981) Multiphasic kinetics for D-glucose uptake by assemblages of natural marine bacteria. Mar Ecol Prog Ser 6:213–222

Bates TS, Kelly KC, Johnson JE, Gammon RH (1995) Regional and seasonal variations in the flux of oceanic carbon monoxide to the atmosphere. J Geophys Res 100: 23093–23101

Bell RT (1993) Estimating production of heterotrophic bacterioplankton via incorporation of tritiated thymidine. In: Kemp PF, Sherr BF, Sherr EB, Cole JJ (eds) Handbook of methods in aquatic microbial ecology. Lewis Publishers, Boca Raton, FL, p 495–503

Butler JH, Jones RD, Garber JH, Gordon LI (1987) Seasonal distribution and turnover of reduced trace gas and hydroxylamine in Yaquina Bay, Oregon. Geochim Cosmochim Acta 51:697–706

Button DK (1998) Nutrient uptake by microorganisms according to kinetic parameters from theory as related to cytoarchitecture. Microbiol Mol Biol Rev 62:636–645

Button DK, Robertson B, Gustafson E, Zhao XM (2004) Experimental and theoretical bases of specific affinity, a cytoarchitecture-based formulation of nutrient collection proposed to supercede the Michaels-Menten paradigm of microbial kinetics. Appl Environ Microbiol 70:5511–5521

Conrad R, Seiler W, Bunse G, Giehl H (1982) Carbon monoxide in seawater (Atlantic Ocean). J Geophys Res 87: 8839–8852

Cornish-Bowden A (1995) Fundamentals of enzyme kinetics. Portland Press, London

d'Anglejan BF, Smith EC (1973) Distribution, transport and composition of suspended matter in the St. Lawrence Estuary. Can J Earth Sci 10:1380–1396

Felip M, Pace ML, Cole JJ (1996) Regulation of planktonic bacterial growth rates: the effects of temperature and resources. Microb Ecol 31:15–28

Gobeil C (2006) Biogeochemistry and chemical contamination in the St. Lawrence estuary. In: Wangersky PJ (ed) Handbook of environmental chemistry, Part H. Springer-Verlag, Berlin, p 121–147

King GM, Weber CF (2007) Distribution, diversity and ecology of aerobic CO-oxidizing bacteria. Nat Rev Microbiol 5:107–118

Koutitonsky VG, Budgen GL (1991) The physical oceanography of the Gulf of St. Lawrence: a review with emphasis on the synoptic variability of the motion. In: Therriault JC (ed) The Gulf of St. Lawrence: small ocean or big estuary? Fisheries and Oceans Canada, Mont-Joli, p 57–90

Le Fouest V, Zakardjian B, Saucier FJ, Starr M (2005) Seasonal versus synoptic variability in planktonic production in a high-latitude marginal sea: the Gulf of St. Lawrence (Canada). J Geophys Res 110, C09012, doi:1029/2004JC002423

Lebel J, Pelletier E (1980) Contribution à l'étude du pH et de la saturation en calcite dans l'estuaire du St-Laurent (Canada). Atmos–Ocean 18:154–167

Lewis DL, Hodson RE, Hwang HM (1988) Kinetics of mixed microbial assemblages enhance removal of highly dilute organic substrates. Appl Environ Microbiol 54:2054–2057

Lovejoy C, Vincent WF, Frenette JJ, Dodson JJ (1993) Microbial gradients in a turbid estuary: application of a new method for protozoan community analysis. Limnol Oceanogr 38:1295–1303

Lovejoy C, Legendre L, Klein B, Tremblay JÉ, Ingram RG, Therriault JC (1996) Bacterial activity during early winter mixing (Gulf of St. Lawrence, Canada). Aquat Microb Ecol 10:1–13

Lovejoy C, Legendre L, Therriault JC, Tremblay JÉ, Klein B, Ingram RG (2000) Growth and distribution of marine bacteria in relation to nanoplankton community structure. Deep-Sea Res II 47:461–487

Moran MA, Miller WL (2007) Resourceful heterotrophs make the most of light in the coastal ocean. Nat Rev Microbiol 5:792–800

Moran MA, Buchan A, González JM, Heidelberg JF and others (2004) Genome sequence of *Silicibacter pomeroyi*

reveals adaptations to the marine environment. Nature 432:910–913

Nieke B, Reuter R, Heuermann R, Wang H, Babin M, Therriault JC (1997) Light absorption and fluorescence properties of chromophoric dissolved organic matter (CDOM), in the St. Lawrence Estuary (Case 2 waters). Cont Shelf Res 17:235–252

Painchaud J, Therriault JC (1989) Relationships between bacteria, phytoplankton and particulate organic carbon in the Upper St. Lawrence Estuary. Mar Ecol Prog Ser 56: 301–311

Painchaud J, Lefaivre D, Therriault JC, Legendre L (1995) Physical processes controlling bacterial distribution and variability in the upper St. Lawrence estuary. Estuaries 18:433–444

Painchaud J, Lefaivre D, Therriault JC, Legendre L (1996) Bacterial dynamics in the upper St. Lawrence estuary. Limnol Oceanogr 41:1610–1618

Shiah FK, Ducklow HW (1994) Temperature regulation of heterotrophic bacterioplankton abundance, production, and specific growth rate in Chesapeake Bay. Limnol Oceanogr 39:1243–1258

Therriault JC, Levasseur M (1985) Control of phytoplankton production in the Lower St. Lawrence Estuary: light and freshwater runoff. Nat Can 112:77–96

Tolli JD, Taylor CD (2005) Biological CO oxidation in the Sargasso Sea and in Vineyard Sound, Massachusetts. Limnol Oceanogr 50:1205–1212

Tolli JD, Sievert SM, Taylor CD (2006) Unexpected diversity of bacteria capable of carbon monoxide oxidation in a coastal marine environment, and contribution of the Roseobacter-associated clade to total CO oxidation. Appl Environ Microbiol 72:1966–1973

Vincent WF, Dodson JJ, Bertrand N, Frenette JJ (1996) Photosynthetic and bacterial production gradients in a larval fish nursery: the St. Lawrence river transition zone. Mar Ecol Prog Ser 139:227–238

Wright RT, Hobbie JE (1965) The uptake of organic solutes in lake water. Limnol Oceanogr 10:22–28

Xie H, Andrews SS, Martin WR, Miller J, Ziolkowski L, Taylor CD, Zafiriou OC (2002) Validated methods for sampling and headspace analysis of carbon monoxide in seawater. Mar Chem 77:93–108

Xie H, Zafiriou OC, Umile TP, Kieber DJ (2005) Biological consumption of carbon monoxide in Delaware Bay, NW Atlantic and Beaufort Sea. Mar Ecol Prog Ser 290:1–14

Xie H, Bélanger S, Demers S, Vincent WF, Papakyriakou TN (2009) Photobiogeochemical cycling of carbon monoxide in the southeastern Beaufort Sea in spring and autumn. Limnol Oceanogr 54:234–249

Yeats PA (1988) Nutrients. In: Strain PM (ed) Chemical oceanography in the Gulf of St. Lawrence. Can Bull Fish Aquat Sci 220, Ottawa, p 29–48

Zafiriou OC, Andrews SS, Wang W (2003) Concordant estimates of oceanic carbon monoxide source and sink processes in the Pacific yield a balanced global 'blue water' CO budget. Global Biogeochem Cycles 17:1015 doi:10.1029/2001GB001638

Zafiriou OC, Xie H, Nelson NB, Najjar RG, Wang W (2008) Diel carbon monoxide cycling in the upper Sargasso Sea near Bermuda at the onset of spring and in midsummer. Limnol Oceanogr 53:835–850

Zapata M, Rodriguez F, Garrido JL (2000) Separation of chlorophylls and carotenoids from marine phytoplankton: a new HPLC method using a reversed phase C_8 column and pyridine-containing mobile phases. Mar Ecol Prog Ser 195:29–45

Zhang Y, Xie H, Fichot C, Chen G (2008) Dark production of carbon monoxide (CO) from dissolved organic matter in the St. Lawrence estuarine system: implication for the global coastal- and blue-water CO budgets. J Geophys Res 113, C12020, doi:10.1029/2008JC004811

Editorial responsibility: Ronald Kiene, Mobile, Alabama, USA

Submitted: March 16, 2009; Accepted: June 22, 2009
Proofs received from author(s): August 30, 2009